Improved strategies for the automatic selection of optimized sets of electrical resistivity tomography measurement configurations

Paul B. Wilkinson, Philip I. Meldrum, Jonathan E. Chambers, Oliver Kuras and Richard D. Ogilvy

British Geological Survey, Natural Environment Research Council, Kingsley Dunham Centre, Keyworth, Nottingham, NG12 5GG, *UK.*
E-mail: pbw@bgs.ac.uk

SUMMARY
Two strategies are presented for obtaining the maximum spatial resolution in electrical resistivity tomography surveys using a limited number of four-electrode measurement configurations. Both methods use a linearized estimate of the model resolution matrix to assess the effects of including a given electrode configuration in the measurement set. The algorithms are described in detail, and their execution times are analysed in terms of the number of cells in the inverse model. One strategy directly compares the model resolution matrices to optimize the spatial resolution. The other uses approximations based on the distribution and linear independence of the Jacobian matrix elements. The first strategy produces results that are nearer to optimal, however the second is several orders of magnitude faster. Significantly however, both offer better optimization performance than a similar, previously published, method. Realistic examples are used to compare the results of each algorithm. Synthetic data are generated for each optimized set of electrodes using simple forward models containing resistive and/or conductive prisms. By inverting the data, it is demonstrated that the linearized model resolution matrix yields a good estimate of the actual resolution obtained in the inverted image. Furthermore, comparison of the inversion results confirms that the spatial distribution of the estimated model resolution is a reliable indicator of tomographic image quality.

Key words: electrical resistivity, inverse theory, numerical techniques, sensitivity, tomography.

1 INTRODUCTION

Over the past decade, geoelectrical surveying techniques have become a popular choice for shallow subsurface investigations. The most widely used of these methods is electrical resistivity tomography (ERT). Recently, several computer controlled multi-electrode ERT systems have become available, which permit the collection of very large data sets that provide coverage of large areas at high data density. Despite the flexible nature of these systems, resistivity data still tend to be collected using traditional electrode arrangements, such as Wenner, Schlumberger or dipole-dipole arrays. These arrays are often a good choice, as they are well understood in terms of their depths-of-investigation (Barker 1989), lateral and vertical resolutions (Barker 1979) and signal-to-noise ratios (Dahlin & Zhou 2004). However, they may not be the most efficient option if the time or number of measurements allowed for the survey is limited, or if a target of particular interest is spatially localized.

Therefore, there is currently much interest in generating sets of electrode configurations that optimize the resolution of the tomographic image for a given number of measurements or in a specified region of the model. The first attempt to do so in resistivity surveying was by Cherkaeva & Tripp (1996), who used weighted sums of pole–pole configurations to produce multi-electrode transmitter and receiver arrays that focused the subsurface current distribution on features at known locations and depths. However, most ERT systems permit at most two current electrodes to be used for a given measurement. Two optimization methods more suited to use with these systems have recently been introduced (Furman *et al.* 2004; Hennig & Weller 2005). Both rely on assessing the sensitivity of given arrays to discrete localized changes in resistivity. The sensitivity distributions are calculated from analytical perturbations (Furman *et al.* 2004) or expressions for the Jacobian matrix elements for the forward problem (Hennig & Weller 2005). Optimization takes place by obtaining weighted sums of these distributions that maximize the sensitivity either evenly across the subsurface model or within a localized region. Summing sensitivity distributions has an intuitive appeal, in that regions of the model with high average sensitivity tend to be well resolved. However, it can only give a correct representation of subsurface resolution in certain limited circumstances. (For example, when the sensitivity distributions have minimal spatial overlap with each other and the regularization constraints are small.) Stummer *et al.* (2004) pioneered a more

accurate approach that uses the sensitivity distributions to calculate an estimate of the model resolution matrix. This provides a measure of how well the observed apparent resistivity data resolve each model cell. They showed that their optimization algorithm produced sets of electrode configurations that out-performed traditional arrays.

In this paper, we present two new ERT optimization strategies, which are both based on finding a limited number of electrode configurations that enhance the model resolution matrix. Of the two, the algorithm that performs better in terms of optimizing the resolution has much longer execution times. The other uses approximations to increase its speed, however manages to achieve similar optimization performance. We compare our methods against that of Stummer *et al.* (2004) in terms of both speed and performance. We also analyse each algorithm's effectiveness at optimizing the model resolution and validate these findings by inverting synthetic data generated using the optimized arrays. In addition, we assess the scaling properties of all three algorithms, quantify the effects of the size of the inverse model on their execution times, and discuss the resulting suitability of each method for different applications.

2 METHOD OVERVIEW

The optimization strategies presented in this paper, all rely on appraisals of the model resolution matrix $\mathbf{R}$. This quantifies the degree to which each resistivity cell in the model can be resolved by the observed data. It is defined by $\mathbf{m}^{\text{fit}} = \mathbf{R}\mathbf{m}^{\text{true}}$ (Menke 1984), where $\mathbf{m}^{\text{fit}}$ is the estimate of the model resistivities determined by the inversion process, and $\mathbf{m}^{\text{true}}$ comprises the true resistivities, which are unknown. If each model cell is perfectly resolved then $\mathbf{R} = \mathbf{I}$, otherwise each row of $\mathbf{R}$ is the constrained least-squares best fit to the corresponding row of $\mathbf{I}$ (Jackson 1972). Strictly, $\mathbf{R}$ can only be defined for linear inverse problems (Friedel 2003). However, despite the fact that the forward problem is non-linear, ERT inversion is typically implemented via an iterative series of linearized steps (Loke & Barker 1995). This permits a first-order estimate of the model resolution matrix to be defined as

$$\mathbf{R} = (\mathbf{G}^{\text{T}}\mathbf{G} + \mathbf{C})^{-1}\mathbf{G}^{\text{T}}\mathbf{G}, \tag{1}$$

where the Jacobian matrix element G_{ij} is the logarithmic sensitivity of the ith measurement to a small change in the resistivity of the jth model cell, and $\mathbf{C}$ contains the damping factors, constraints and spatial filters that regularize the inversion (Loke *et al.* 2003). Our optimization procedures attempt to maximize the matrix elements on the leading diagonal of $\mathbf{R}$. We denote these elements $R(j)$ and call them the 'model resolution', noting that they are also sometimes referred to as the 'model importance'. Since $\mathbf{R}$ is the least-squares fit to $\mathbf{I}$, the model resolution lies in the range $0 \leq R(j) \leq 1$. It provides a simple measure of how well the jth resistivity model cell is resolved by the data (0 being unresolved and 1 perfectly resolved).

For a system of N electrodes, the comprehensive measurement set contains $N(N-1)(N-2)(N-3)/8$ non-equivalent four-electrode configurations when reciprocity is taken into account (Xu & Noel 1991). It is likely that this set will contain configurations that reduce the stability of the inversion, such as those of the Wenner-γ type and others with large geometrical factors. These can be discarded before the optimization process begins, leaving a set S_{c} containing n_{c} configurations. Suppose that one wishes to find the subset of n_{b} measurements from S_{c} that, by some measure, provides the optimal

model resolution. Since there are $\frac{n_{\text{c}}!}{n_{\text{b}}!(n_{\text{c}}-n_{\text{b}})!}$ such combinations, and since n_{c} scales as $O[N^4]$, there is no practical possibility of testing them all. One could try a global optimization technique, such as simulated annealing or a genetic algorithm. However, the sheer number of possible combinations and the lack of an obvious algorithm for producing beneficial test combinations would almost certainly limit its effectiveness.

A more practical approach is to use local optimization. The most effective method would be to select a small initial base set, then test every other configuration by recalculating R for the base set *plus* that particular configuration. The best configuration would then be added to the base set for the next iteration, and the process would be repeated until the set contained the required number of configurations. However, each step would require $O[N^4]$ calculations of R, and each of these calculations would require a matrix inversion, which is an $O[m^3]$ process, where m is the number of model cells. These unfavourable scaling properties make this form of local optimization far too inefficient for practical use. However, several modifications can be made so that it retains most of its efficacy whilst drastically improving its efficiency. Since R does not tend to change rapidly after the first few steps, it is not necessary to recalculate it for the add-on configurations every time. In the intervening iterations, it is sufficient to check that the sensitivity distribution of the configuration being tested has a degree of orthogonality to those that have already been added (Stummer *et al.* 2004; Menke 1984). Since this check is an $O[m]$ process, this modification leads to a considerable increase in speed. When R does need to be recalculated, this can be done by updating the model resolution of the base set using a Rank-1 correction based on the Sherman–Morrison formula (Press *et al.* 1992). This replaces the $O[m^3]$ matrix inversion with an $O[m^2]$ process, giving a further large performance benefit. The local optimization method, with these two modifications, is the basis of our first strategy ('Compare R'). It is still rather slow, taking several hours on a 3 GHz desktop PC for a realistic 2.5-D ERT problem, however, it does give very good results.

The above method was developed as a more effective version of the strategy of Stummer *et al.* (2004). In their paper, each configuration is ranked by a 'Goodness Function' that attempts to assess the effects of its addition to the base set without calculating R explicitly. This replaces the $O[m^3]$ matrix inversions with several $O[m]$ calculations and is, therefore, much faster than the 'Compare R' approach, taking only a few minutes to run for the same problem. However, their method, which we denote the 'Original GF' algorithm, is also significantly less effective at optimizing the model resolution. We have improved on their approach to create the 'Modified GF' strategy, which not only gives results that are closer to those obtained from 'Compare R', but is faster still than 'Original GF'.

3 CONFIGURATION ASSESSMENT

3.1 Strategy 1–Compare R

This is the most computationally intensive approach of the three strategies. Each possible configuration to be added to the base set is ranked in terms of $\frac{1}{m}\sum_{j=1}^{m}\frac{R_{\text{t}}(j)}{R_{\text{b}}(j)}$, where R_{t} is the resolution of the base set plus the test configuration and R_{b} is the resolution of the base set. The finesse in the method involves using the Sherman–Morrison Rank-1 update to calculate R_{t} from the known R_{b}, rather than explicitly from eq. (1). Briefly, if $\mathbf{g}$ is the m element vector containing the logarithmic sensitivities of the test configuration and $\mathbf{R}_{\text{b}}$ has already been calculated using eq. (1), then the matrices are

updated as follows:

$$\mathbf{G}^T\mathbf{G} \rightarrow \mathbf{G}^T\mathbf{G} + \mathbf{g} \otimes \mathbf{g},$$

$$(\mathbf{G}^T\mathbf{G} + \mathbf{C})^{-1} \rightarrow (\mathbf{G}^T\mathbf{G} + \mathbf{C})^{-1} - \frac{\mathbf{z} \otimes \mathbf{z}}{1+\mu}, \quad (2)$$

where $\mathbf{z} = (\mathbf{G}^T\mathbf{G} + \mathbf{C})^{-1}\mathbf{g}$, $\mu = \mathbf{g} \cdot \mathbf{z}$ and $\mathbf{a} \otimes \mathbf{b}$ denotes the matrix multiplication of $\mathbf{a}$ and $\mathbf{b}^T$. Each step in this process scales as $O[m^2]$ or better, and the final calculation of R_t is also $O[m^2]$ if only the leading diagonal of $\mathbf{R}_t$ is calculated.

Many configurations are added to the base set at each iteration. The first is the highest ranked configuration, represented by the sensitivity vector $\mathbf{g}_1$. The next highest ranked, $\mathbf{g}_2$, is then added only if it is deemed to have a suitable degree of orthogonality to the first. This is assessed by calculating $|\mathbf{g}_1 \cdot \mathbf{g}_2|/(|\mathbf{g}_1| |\mathbf{g}_2|)$ and checking that it is less than a specified limit. This procedure is repeated until the desired number of extra configurations has been appended to the base set, with each configuration being checked against those that were previously added on this iteration only.

3.2 Strategy 2—Original GF

Full details of the original goodness function are given in Stummer *et al.* (2004). In brief, the ith add-on configuration is ranked by a goodness function defined by

$$F_i = \sum_{j=1}^{m} \frac{|G_{ij}|}{G_j^{sum}}\left[1 - \frac{R_b(j)}{R_c(j)}\right], \quad (3)$$

where

$$G_j^{sum} = \frac{1}{n_c}\sum_{k=1}^{n_c}|G_{kj}| \quad (4)$$

and R_c is the model resolution of the comprehensive set. The bracketed term in eq. (3) selects configurations that improve regions of the model that are poorly resolved by the base set. G_j^{sum} provides a normalization factor by summing the absolute sensitivities for the jth model cell of all configurations in the comprehensive set. This ensures that the goodness function gives equal preference to improving the resolution in all regions of the model, regardless of their relative sensitivity.

As with the 'Compare R' approach, multiple configurations are tested for inclusion in the base set at each iteration. In this strategy, the orthogonality check is performed against the entire base set, not just the configurations that have been added on this pass. This means that, if the add-on configuration fails this test against some configuration in the base set, then it will also fail at every future iteration (since that configuration will remain in the base set). Therefore, any failing add-on configurations are discarded to save time in subsequent iterations. However, if the orthogonality test is too strict, it is possible to discard all the add-on configurations, thereby causing the algorithm to halt prematurely.

3.3 Strategy 3—Modified GF

The modified goodness function follows a similar approach to the original. Each configuration is ranked by

$$F_i = \sum_{j=1}^{m} \frac{G_{ij}^2}{\left(G_j^{sum}\right)^2}\left(1 - \frac{R_b(j)}{R_c(j)}\right)^{1/2}, \quad (5)$$

where

$$G_j^{sum} = \frac{1}{n_b}\sum_{k=1}^{n_b}|G_{kj}|. \quad (6)$$

The changes between the modified and original goodness functions are pragmatic in nature, having been found to be beneficial on the basis of numerical tests involving several different subsurface geometries. The G_j^{sum} term now only sums over the n_b configurations in the base set. Its purpose has been changed so that it gives high weighting to add-on configurations that are orthogonal to the base set, and this effect is increased by the squared terms in eq. (5). Since low values of G_j^{sum} tend to imply poor resolution of the jth model cell, these modifications can overemphasize the importance of configurations with sensitivity distribution that are strongly localized in poorly resolved regions of the model. This can have the side-effect that other useful configurations, which provide more uniform improvements to the model resolution, are often ignored. Therefore, the bracketed term in eq. (5), which has the purpose of improving the same poorly resolved regions, has had its exponent reduced to restore the balance. The overall effect of the modifications is that add-on configurations are chosen which improve the resolution whilst *simultaneously* having a high degree of orthogonality to the base set. This means that it is only necessary to perform the separate orthogonality test against the configurations that have been added during this iteration, rather than against the whole base set. This substantially reduces the amount of time spent performing these checks, and removes the possibility of running out of add-on configurations.

4 PERFORMANCE TESTS

We have tested each of the strategies using a 2.5-D geometry which matches that used in Stummer *et al.* (2004). This consists of 30 electrodes positioned at 5 m spacings and 16 exponentially increasing depth levels in the model, giving a total of $m = 464$ resistivity model cells. All the Wenner-γ configurations and others with geometrical factors larger than 5500 m were discarded, leaving a comprehensive set S_c containing $n_c = 51\,373$ unique configurations. The initial base set S_b was a sparse dipole–dipole array comprising $n_b = 147$ configurations with an 'a-spacing' of 1 and 'n-levels' of $1 \rightarrow 6$. At each iteration an extra $0.09n_b$ configurations were added to S_b, and n_b was updated to $1.09n_b$.

The Jacobian matrix $\mathbf{G}$ contains the logarithmic sensitivity of each configuration to changes in the model resistivities. It was calculated using the adjoint field approach (Park & Van 1991), which is valid for arbitrary resistivity distributions. To ensure that the generated sets of configurations would be applicable to general resistivity surveys, we assumed no prior knowledge of the resistivity distribution. Therefore, we chose to use a homogeneous half-space, which increased the speed and simplicity of the sensitivity calculations. As an aside, in this situation the adjoint field method also has a particularly simple physical interpretation (see Appendix A).

In addition to the unknown resistivity distribution, the final constraint matrix cannot be determined before the inversion is performed. This is due to the iterative nature of the non-linear inverse resistivity problem; the inversion algorithms tend to change the constraints at every iteration to maintain stability and maximize image resolution. Fortunately the optimization strategies all rank the additional configurations in terms of one model resolution distribution divided or normalized by another. Therefore, they are relatively insensitive to the detailed structure of these distributions, and hence also to the constraint matrix, providing that the model resolutions are physically reasonable (Stummer *et al.* 2004). Consequently, we used a simple damping constraint $\mathbf{C} = \lambda\mathbf{I}$ with $\lambda = 2.5 \times 10^{-6}$, which was chosen so that the model resolution, R_c, of the comprehensive measurement set was small ($R_c \sim 0.05$) at a depth of
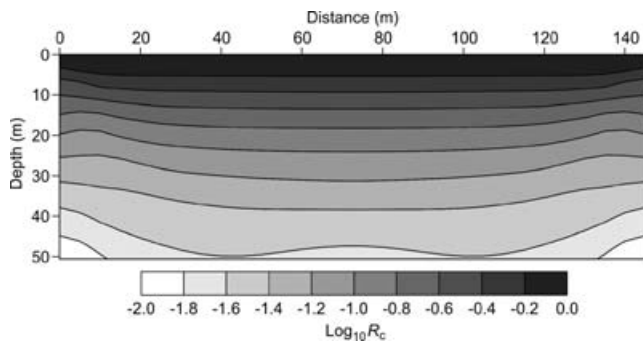
Figure 1. Logarithm of the model resolution R_c for the comprehensive set of configurations.

~30 m. This depth is the typical maximum median depth of investigation for four-electrode configurations on an array of 145 m length (Barker 1989). The distribution of R_c is shown in Fig. 1 on a logarithmic scale. Its spatial dependence appears realistic since it exhibits the typical, approximately exponential, decrease of resolution with depth.

Each algorithm was run for 40 iterations, producing a set of 4368 configurations. The upper limit on orthogonality was chosen separately to give the best possible results for each algorithm. Therefore, this limit is slightly different for each, being 0.97 for 'Compare R', 0.98 for 'Original GF' and 0.95 for 'Modified GF'. The outputs of each strategy are shown in Fig. 2 as plots of the spatial distribution of the *relative* model resolution, R_r. This is defined as the model resolution of the optimized set divided by that of the comprehensive set ($R_r = R_b/R_c$). The colour scale ranges from white

($R_r = 0$), through the visible spectrum from blue to red, to black ($R_r = 1$). The best possible relative model resolution distribution would be provided by the comprehensive set, and would, therefore, equal 1 (black) throughout the model space. Note that this means that the model resolution would be as shown in Fig. 1, it does not imply that the model resolution would be uniformly good everywhere. The plots in Fig. 2 show R_r at six different stages of the optimization process (iteration numbers 1, 8, 16, 24, 32 and 40). Qualitatively it can be seen that the model resolution improves with increasing iteration number for each of the optimization strategies. It should also be clear from Fig. 2 that, by iteration 40, the 'Compare R' strategy has produced the best distribution of R_r, whereas the performance of 'Original GF' is noticeably worse. However, the results of the 'Modified GF' algorithm appear to be nearly as good as those of 'Compare R'. The execution times for the algorithms were 6.0 hours for 'Compare R', 6.3 minutes for 'Original GF' and 3.9 min for 'Modified GF'.

A more quantitative measure of the performance of each method is presented in Fig. 3. The graphs show the average value of the relative model resolution, $S = \frac{1}{m} \sum_{j=1}^{m} R_r(j)$, plotted against the iteration number for 'Compare R' (blue line), 'Modified GF' (red line) and 'Original GF' (green line). From these graphs, it can be clearly seen that the 'Compare R' strategy is the most effective, producing a final average resolution of $S = 0.94$, closely followed by 'Modified GF' ($S = 0.92$), with the least effective being 'Original GF', which produced $S = 0.84$. It should be emphasized that these optimized sets contain only 4368 configurations, or 8.5 per cent of the total number available. Despite this, they achieve average model resolutions comparable with that of the comprehensive set ($S = 1.00$).
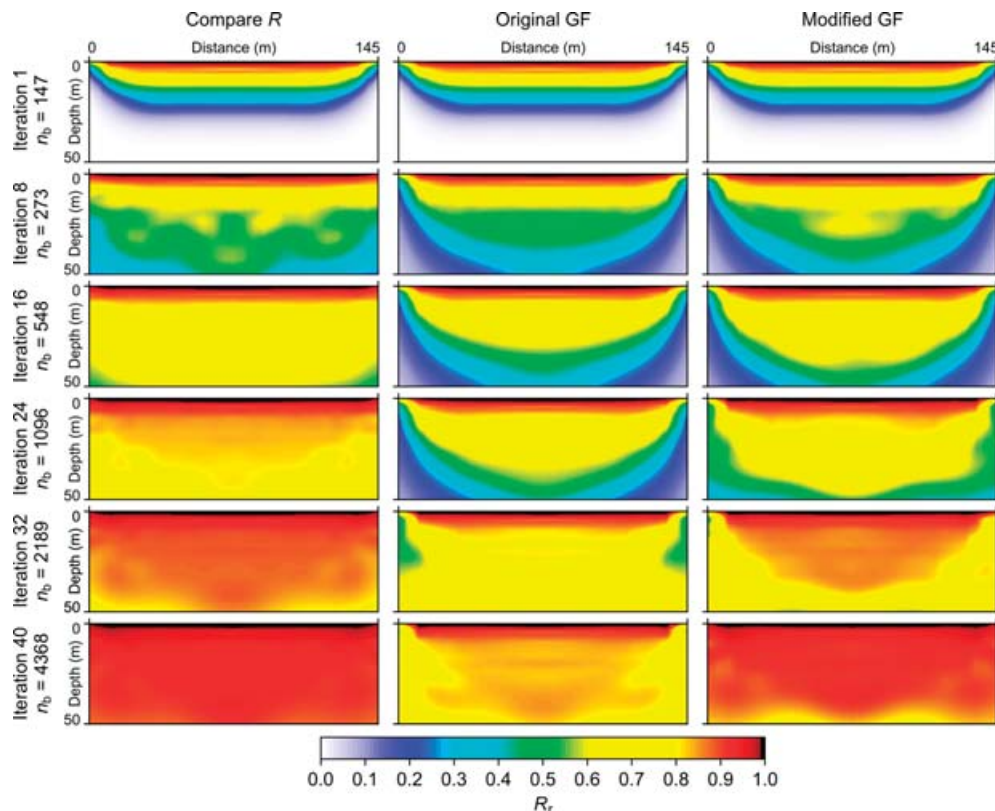

Figure 2. Relative model resolutions R_r at six different stages of the optimization process for each strategy. Each column shows the results of a different optimization strategy, with the iteration number and number of configurations in the optimized sets increasing down the page.
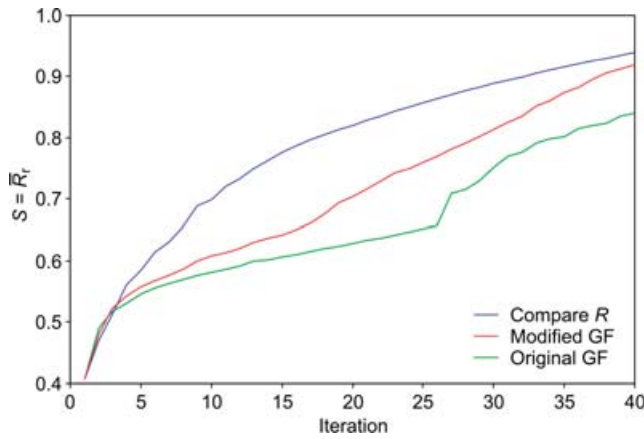
Figure 3. Average relative model resolution as a function of iteration number for each of the three optimization strategies.

As with Stummer *et al.* (2004), we find that the largest improvements in R_r are due to the inclusion of asymmetric dipole–dipole configurations. Our implementation of their 'Original GF' algorithm exhibits very similar behaviour to that which they reported. The algorithm initially selects only dipole–dipole type configurations, in our case for the first 25 iterations. After this point, nested configurations (i.e. the C1-P1-P2-C2 type) are chosen more and more frequently, with the numbers of both types projected to be roughly equal (about 3000 of each) at the 43rd iteration. The 'Compare R' method produces somewhat different behaviour, with dipole–dipole and nested configurations being added in approximately the same ratio (∼4:1) at each iteration. The 'Modified GF' approach is similar, but the proportion does change slightly, from ∼11:1 initially to ∼9:1 at the 40th iteration. Compared to 'Original GF', both of our new approaches tend to utilize more of the asymmetric dipole–dipole configurations and select them earlier in the optimization process.

5 INVERSION RESULTS

Having obtained distributions of R_r from the three optimization strategies, it is desirable to invert data obtained from the respective sets of configurations to test how well each set performs against known targets. This is to give confidence that assessing the distribution of R_r is a good way to predict the inversion performance of a given configuration set. To this end we have tested each set against three synthetic models, one with four resistive prisms of $\rho = 100\,\Omega$m buried at different depths in a background with $\rho = 10\,\Omega$m (Fig. 4a), another with only the deepest of the four prisms (Fig. 4e), and a third with both conductive and resistive structures (Fig. 5a). The data were calculated using the Res2DMod software with a finite-difference forward modelling algorithm. They were inverted using the companion Res2DInv program using the same model cell discretization and an l_1-norm (robust) model constraint (Loke *et al.* 2003). The finite-element method was used within Res2DInv to avoid having the same combination of discretization and modelling algorithm in the forward and inversion processes.

The inverted images for the four-prism model are shown in Figs 4(b–d) for the 'Compare R', 'Original GF' and 'Modified GF' strategies, respectively. We assess the resolution quality by the degree to which a localized resistivity structure in the inverted image is contained within the boundary of the corresponding prism in the forward model. We also take into account the degree to which the resistivity contrast in the forward model is reflected in the inversion.

In these qualitative terms, it can easily be seen that the prisms are best resolved by the 'Compare R' configurations, then by 'Modified GF', and least well by 'Original GF'. This agrees with what would be expected from the degree of optimization of the respective R_r distributions.

These assessments can be quantified by calculating the average resistivity value within the outlines of the prisms. The closer each prism is to being perfectly resolved, then the nearer the average value would be to 100 Ωm. The average resistivity values are shown adjacent to each prism in Figs 4(b–d). By this measure, the best resolution for all four prisms is obtained with the 'Compare R' algorithm. With the exception of the deepest prism, the next best results are obtained using 'Modified GF', whilst 'Original GF' gives the poorest resolution. Although the deepest prism has a slightly higher average resistivity using the 'Original GF' strategy as opposed to the 'Modified GF', its structure is not actually resolved at all in either image. We have examined both of these images using much higher resolution contouring than shown in Fig. 4. This has confirmed that, in contrast to the 'Compare R' image, neither contains an isolated resistivity maximum in the vicinity of this prism. The associated average values merely reflect the spatial trends of the resistivity over a much larger area.

Although 'Compare R' managed to resolve a weak localized resistivity maximum in the vicinity of the deepest prism, it is clear that the resolution in this region is poor using any of the three strategies. Therefore, to assess their resolving capabilities more accurately at these depths, we have repeated the exercise using a forward model containing only the deepest prism (Fig. 4e). The inverted images for this single-prism model are shown in Figs 4(f–h) using a compressed colour scale. With the same assessment criteria as before, the 'Compare R' scheme performs the best, showing some localized structure and the greatest resistivity contrast against the background. The capabilities of the 'Original GF' and 'Modified GF' schemes are similar, but the 'Modified GF' is the better of the two, resolving a faint localized structure where the 'Original GF' produces none, and also producing a slightly higher resistivity contrast. These observations are corroborated by the average resistivity value, which is highest for 'Compare R', and marginally higher for the 'Modified GF' than the 'Original GF'.

It is also possible to compare the spatial resolution measured directly from the inverted images with an estimate of the radius of resolution obtained from R. Using the results for 'Compare R' as an example, we defined the edge of the prism in the inverted image to be at 11.8 Ωm, which is the centre contour between the maximum and background resistivities. We measured the spatial resolution as the distance between this contour and the edges of the prism in the forward model, obtaining a value of ∼9.2 m. At the midpoint of the prism, the estimated model resolution is $R \sim 0.035$. The radius of resolution, defined by Friedel (2003), is given by

$$r = \sqrt{\frac{A}{\pi R}}, \tag{7}$$

where $A = 12.5\,\text{m}^2$ is the area of the model cell at the prism midpoint. This gives an estimated radius of resolution of $r \sim 10.7$ m. The good agreement between these two estimates of spatial resolution further validates the use of the simple damping constraint in eq. (1), and gives added confidence in the use of model resolution estimates to predict inversion performance.

Whilst the forward and inverse models involving resistive prisms illustrate the close correspondence between R and the spatial resolution, it is also helpful to examine the performance of the same optimized arrays against a more general model. To this end, we
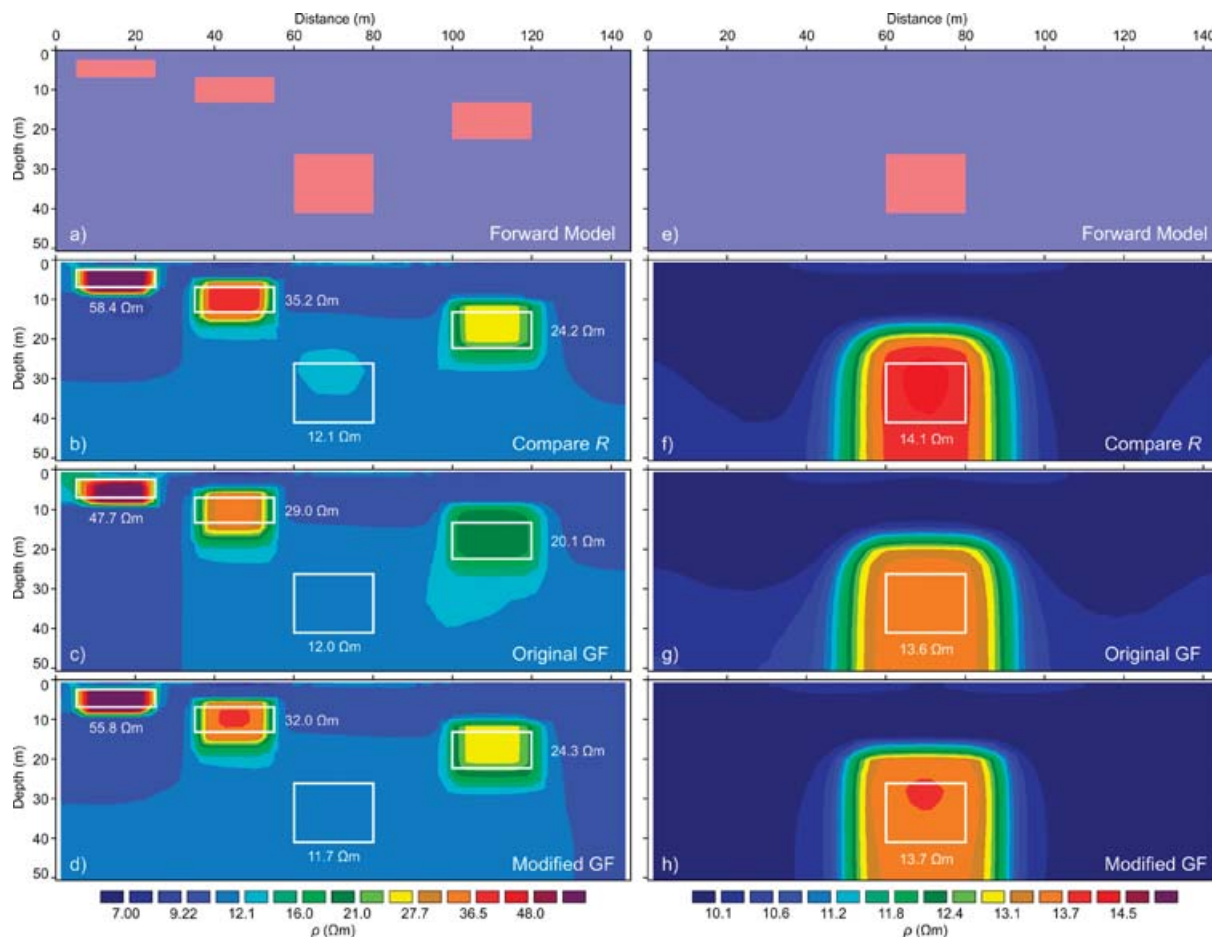
Figure 4. Forward models (a) and (e) showing the locations and sizes of resistive prisms ($\rho = 100 \, \Omega$ m, light red) embedded in an otherwise uniform background ($\rho = 10 \, \Omega$m, light blue). Also shown are inverted images obtained from forward modelled synthetic data using optimized sets of configurations generated with (b) and (f) 'Compare R', (c) and (g) 'Original GF', and (d) and (h) 'Modified GF'. The displayed average resistivity values relate to the regions of the inverted images bounded by the prisms.

consider the model used by Stummer *et al.* (2004), which consists of a conductive overburden, a resistive prism and an inhomogeneous conductive prism (Fig. 5a). For ease of comparison we have adopted their colour scale and block display for Fig. 5. It should be noted that, when comparing the results of the two papers, we have used an l_1-norm model constraint, which has the effect of improving the recovered blocky geometry of the model, but also reduces the peak resistivity or conductivity contrasts that are obtained. By inspecting Figs 5(b–d), it is clear that each of the three algorithms has resolved the two prisms and the overburden. Marginally better resistivity contrasts are obtained with 'Compare R' (Fig. 5b) for the conductive prism, and with 'Modified GF' (Fig. 5d) for the resistive prism. However, there is little quantitative difference, as evidenced by the similar average resistivity values obtained with each algorithm. More importantly, each of the new strategies significantly improves on the resistivity contrasts achieved with the 'Original GF' method (Fig. 5c).

6 CONCLUSIONS

We have proposed two new local optimization strategies that, for a given limited number of four-electrode configurations, provide near-optimal subsurface resolution for ERT surveys. Both algorithms use

a linearized first-order estimate of the model resolution to assess the suitability of the electrode configurations. One approach, 'Compare R', calculates the effects of adding new configurations directly by updating the model resolution matrix. The other method, 'Modified GF', uses a goodness function to estimate which new configurations would be beneficial to include.

We compared these schemes with the 'Original GF', a previously published algorithm that uses a similar approach. Our tests indicate that 'Compare R' produces the closest to optimal subsurface distribution of model resolution. However, this algorithm is slow and scales unfavourably with the number of resistivity cells in the model. The 'Original GF' method is at least an order of magnitude faster, however, its results exhibit notably poorer resolution. However, our 'Modified GF' runs faster still and produces model resolutions that are much closer to those obtained by the 'Compare R' method.

The estimate of model resolution was calculated on the basis of a homogeneous half-space so that the results would not be specific to any particular subsurface resistivity distribution. This had the additional benefit of increasing the speed and simplicity of the Jacobian matrix calculations. Despite these assumptions, tests involving the inversion of synthetic data derived from forward models with resistivity contrasts of 10:1 demonstrated that the distribution of the estimated model resolution was a reliable indicator of the quality of the final inverted image. Both qualitative and quantitative
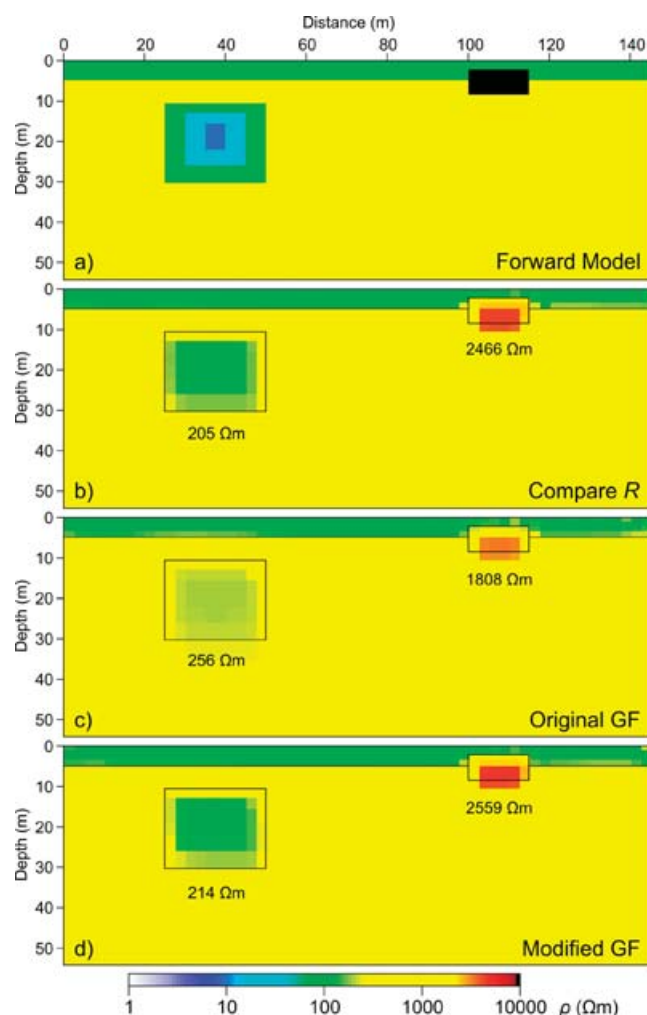
Figure 5. (a) Forward model used in Stummer *et al.* (2004), showing the locations of conductive and resistive prisms and a conductive overburden in an otherwise uniform half-space ($\rho = 1000\,\Omega$m, yellow). Also shown are inverted images obtained from forward modelled synthetic data using optimized sets of configurations generated with (b) 'Compare R', (c) 'Original GF' and (d) 'Modified GF'. The displayed average resistivity values relate to the regions of the inverted images bounded by the prisms.

assessments of the inverted images showed that the best results were obtained with the 'Compare R' strategy closely followed by our 'Modified GF', whereas the poorest resolution was produced by the 'Original GF'. These findings were supported by further tests on a more general model involving both conductive and resistive prisms and a conductive overburden.

By applying a spatial weighting function to the model resolution distribution, it would not be difficult to adapt these procedures to target a specified region of the subsurface (Hennig & Weller 2005; Furman *et al.* 2004). Our scaling analysis suggests that, due to its long execution times, 'Compare R' is likely to be used only in the preparation stages for a field survey, and would, therefore, require prior knowledge of the target areas and geometries. However, the 'Modified GF' method is probably fast enough that it could be used for real-time array optimization. It could, therefore, form the basis of an adaptive time-lapse electrical imaging system. This would use feedback from the resistivity image to determine time-dependent weighting functions for the next inversion, automatically optimiz-

ing the spatial resolution for time-lapse tomographic imaging of dynamic subsurface processes.

REFERENCES

Barker, R.D., 1979. Signal contribution sections and their use in resistivity studies, *Geophys. J. R. astr. Soc.,* **59,** 123–129.

Barker, R.D., 1989. Depth of investigation of collinear symmetrical four-electrode arrays, *Geophysics,* **54,** 1031–1037.

Cherkaeva, E. & Tripp, A.C., 1996. Optimal survey design using focused resistivity arrays, *IEEE Trans. Geosci. Remote Sens.,* **34,** 358–366.

Dahlin, T. & Zhou, B., 2004. A numerical comparison of 2-D resistivity imaging with 10 electrode arrays, *Geophys. Prospect.,* **52,** 379–398.

Friedel, S., 2003. Resolution, stability and efficiency of resistivity tomography estimated from a generalized inverse approach, *Geophys. J. Int.,* **153,** 305–316.

Furman, A., Ferré, T.P.A. & Warrick, A.W., 2004. Optimization of ERT surveys for monitoring transient hydrological events using perturbation sensitivity and genetic algorithms, *Vadose Zone J.,* **3,** 1230–1239.

Hennig, T. & Weller, A., 2005. Two dimensional object orientated focusing of geoelectrical multi-electrode measurements. *Proceedings of the 11th meeting of the EAGE Near Surface Geophysics Conference*, Palermo, Italy.

Jackson, D.D., 1972. Interpretation of inaccurate, insufficient and inconsistent data, *Geophys. J. R. astr. Soc.,* **28,** 97–109.

Loke, M.H. & Barker, R.D., 1995. Least-squares deconvolution of apparent resistivity pseudosections, *Geophysics,* **60,** 1682–1690.

Loke, M.H., Acworth, I. & Dahlin, T., 2003. A comparison of smooth and blocky inversion methods in 2-D electrical imaging surveys, *Explor. Geophys.,* **34,** 182–187.

Lorrain, P., Corson, D.R. & Lorrain, F., 1988. *Electromagnetic Fields and Waves*, W.H. Freeman & Co, New York.

Menke, W., 1984, *Geophysical data analysis: Discrete Inverse Theory*, Academic Press, London.

Park, S.P. & Van, G.P., 1991. Inversion of pole–ipole data for 3-D resistivity structure beneath arrays of electrodes, *Geophysics,* **56,** 951–960.

Press, W.H., Teukolsky, S.A., Vetterling, W.T. & Flannery, B.P., 1992. *Numerical Recipes in C: The Art of Scientific Computing*, 2nd edn, Cambridge University Press, Cambridge.

Stummer, P., Maurer, H. & Green, A.G., 2004. Experimental design: Electrical resistivity data sets that provide optimum subsurface information, *Geophysics,* **69,** 120–139.

Xu, B. & Noel, M., 1991. Archaeological investigation by electrical resistivity tomography: a preliminary study, *Geophys. J. Int.,* **107,** 95–102.

APPENDIX A: PHYSICAL INTERPRETATION OF SENSITIVITY CALCULATIONS

The derivation of the adjoint method used to calculate the Jacobian matrix elements is mathematically dense (Park & Van 1991) and does not readily give insight into the physical origins of the form of the sensitivity function. However, when the subsurface resistivity distribution is homogeneous, the sensitivity does have a simple physical interpretation; the change in potential due to a small
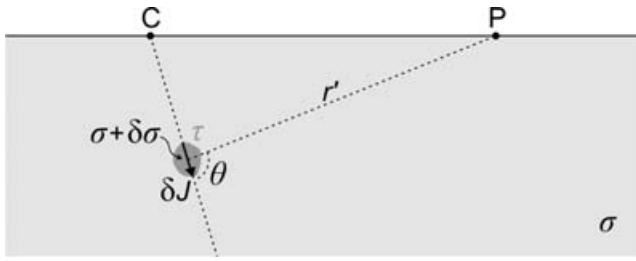
Figure A1. A background medium of uniform conductivity σ incorporates a small volume τ with conductivity $\sigma + \delta\sigma$. In the electric field of a current source C this causes a dipolar perturbation current density of δJ at an angle θ and distance r' to the field point P.

localized resistivity perturbation is due to the change in dipolar current density flowing in the perturbed region.

To demonstrate this, we consider a homogeneous half-space of conductivity σ containing a small volume τ in which the conductivity is $\sigma + \delta\sigma$ (Fig. A1). If the perturbation is weak, then the electric field $\mathbf{E}$ in τ can be assumed to be unchanged (this is equivalent to the Born Approximation in scattering theory). The field $\mathbf{E}$, due to the current electrode C, produces a dipolar current flow through the volume τ. The change in the dipolar current density caused by the conductivity perturbation is $\delta\mathbf{J} = \mathbf{E}\delta\sigma$. In turn, this extra current density changes the potential at P by

$$\delta V = \int_\tau \frac{\delta J \cos\theta}{2\pi\sigma r^2} d^3\mathbf{r} \tag{A1}$$

(Lorrain *et al.* 1988), where $\mathbf{r}$ is a position vector within τ, and r' and θ are the distance and angle from τ to P, respectively. The magnitude of the electric field of a notional unit current pole located at P would be $E' = \frac{1}{2\pi\sigma r'^2}$. Therefore

$$\delta V = \int_\tau E\delta\sigma E' \cos\theta d^3\mathbf{r}$$
$$= \int_\tau -\delta\sigma \mathbf{E} \cdot \mathbf{E}' d^3\mathbf{r}, \tag{A2}$$

where the minus sign arises since $\mathbf{E}'$ is antiparallel to $\mathbf{r}'$. Rearranging eq. (A2) slightly in terms of resistivity ρ gives

$$\delta V = \frac{\delta\rho}{\rho^2} \int_\tau \mathbf{E}' \cdot \mathbf{E} d^3\mathbf{r}, \tag{A3}$$

which is the result found in Park & Van (1991).